Title: Development of a Heat Transfer Finite Element Model to Study the Thermal Performance of an Anglian Home Improvements Conservatory Installation

For: Anglian Home Improvements

By: James Dean

Reference: DPC/003/Glazing/Draft6

doubleprecision

fea and multiphysics

Technical Review Summary

Technical work undertaken by: Dr. James Dean,
Senior Consultant, Double Precision Consultancy Ltd.

Date: 08/04/16

Technical review undertaken by: Matthew Cubitt,
Design Engineer, Anglian Home Improvements Ltd.

.....

Date: .....

Contents

1.0 Introduction 1

2.0 Radiation 2

2.1 Radiation and Emission 2

2.2 Reflection, Absorption and Transmission of Solar Radiation 3

3.0 Case Study Overview

3.1 Case 1 4

3.2 Case 2 5

3.3 Case 3 5

4.0 Model Build

4.1 Geometry 6

4.2 Geometry Simplifications 6

4.3 A Protocol for Maintaining Component U-values in Simplified Geometries 7

4.4 Material Properties 8

4.5 Boundary Conditions 8

4.5.1 Solar Radiation 8

4.5.2 Ambient Temperature Conditions 9

4.5.3 Convective Heat Transfer 9

4.5.3.1 External 9

4.5.3.2 Internal 9

4.5.4 Radiation Heat Transfer 10

4.5.4.1 Transmission of Energy 10

4.5.5 Underground Temperature 11

4.5.6 Cloud Cover 11

5.0 Results

5.1 Internal Room Temperatures 12

5.1.1 January 12

5.1.2 July 12

5.1.3 Internal Room Temperature Ranking 12

5.2 The Effectiveness of the Low-ε Coating 16

5.3 Correlation with Measured Internal Temperature Data 17

5.4 Cloud Cover Corrections 18

5.5 External Rafters Temperature 18

6.0 Conclusions 19

1 Introduction

Solar Heat Gain (SHG) is a term that describes the increase in temperature that occurs within an enclosed building due to solar radiation. A classic example of SHG in action is in the common garden greenhouse where incident, short wavelength solar radiation is transmitted through the glass while internally emitted, long wavelength radiation, is retained inside.

SHG can be quantified using the Solar Heat Gain Coefficient (SHGC or 'g' value), which is a measure of the fraction of incident solar radiation that contributes to SHG. These contributions can be direct (transmittance – i.e. though glazing), and indirect (i.e. via absorption of radiation followed by emittance). It therefore follows that the SHGC will be sensitive to the characteristics of the window assembly, including the type, number and thickness of the window panes, the window pane spacing, the type of gas between the panes, the thermal characteristics of the frame and, of course, the thermal characteristics of the rest of the room. Another important energy-performance metric (in addition to the SHGC) is commonly used within the industry – the U-value. The U-value is a measure of heat transmission, expressed in $W\ m^{-2}\ K^{-1}$. It is a measure of the *rate* of energy transmission per unit area per unit temperature difference, where a high U-value implies a high rate of heat transmission and a low U-value implies a low rate of heat transmission.

It is useful then to consider the requirements for year-round solar control inside conservatories and to express these requirements in terms of the SHGC and the U-value. For instance, during summer months, conservatories can become uncomfortably hot if the SHG is high. In contrast, during the winter months, door and window assemblies with high SHGCs and low U-values are preferable since this combination helps maintain warm internal temperatures (thereby reducing levels of energy consumption). Furthermore, during summer months the levels of light transmittance through conservatory glazing should be tailored so that the risk of glare is low, yet the most effective methods for minimising glare (i.e. tints and films) can adversely affect the levels of light transmittance during winter.

To reconcile these competing requirements, manufacturers have adopted increasingly sophisticated coatings (often sputtered) that are low-ε and/or spectrally-selective and/or tinted. Since the costs associated with the deposition or application of these coatings are expensive, Anglian have recently attempted to identify glazing types that are suitable for use in conservatories all year round – i.e. those optimised for good solar control in summer, whilst also allowing for a degree of solar gain and good insulation in winter. The ultimate goal is to optimise the comfort levels inside the conservatory throughout the year. Two such glasses were identified. These were (a) SunGuard HP 50/32 and (b) SunGuard HP 60/40.

In order to test the performance of the SunGuard glazing options a conservatory installation in Woking was retro-fitted with the SunGuard glazing options. The windows on the roof were fitted with HP 50/32 and the windows around the side were fitted with HP 60/40. The glazing that was replaced in the trial installation was bronze-tinted, anti-sun in the roof and clear in the walls. Venetian blinds (controlling solar gain and glare) were removed from the conservatory when the glazing was replaced. However, after ~9 months (and during the first summer period), evidence emerged of the foil peeling on the upper west facing side of the conservatory. Soon after, some peeling on the east-facing side and internally was also observed. An internal temperature measurement in August 2014 read 38°C, while the inner wall glass was "hot to the touch". Evidence of foil peeling was therefore attributed (tentatively) to the change in the glazing type. The packages of work described in this report were designed to confirm (or otherwise) this hypothesis using heat transfer finite element analyses.

2 Radiation

2.1 Radiation and Emission

Two types of radiation are considered in this report – radiation emitted by the sun at short wavelengths (<2.5 µm) and radiation emitted by objects on Earth at long wavelengths (>2.5 µm).

The sun emits radiation at short wavelengths because of its very high surface temperature. In fact, the spectrum of radiation emitted by the sun looks very much like the radiation spectrum of a blackbody that is radiating at a temperature of 5800 K – such as that shown in Fig.1 (note that the radiative flux has been scaled in order to fit the curve on the graph). Nearly all of the emitted energy is emitted at wavelengths (λ) that are less than 2.5 µm.

In contrast, most objects on Earth are much cooler than the sun (say 273 K – 350 K) and emit radiation at longer wavelengths. For comparison, the radiation spectrum from a cool object is also shown in Fig.1 (red curve). The spectrum is for a blackbody at 293 K.

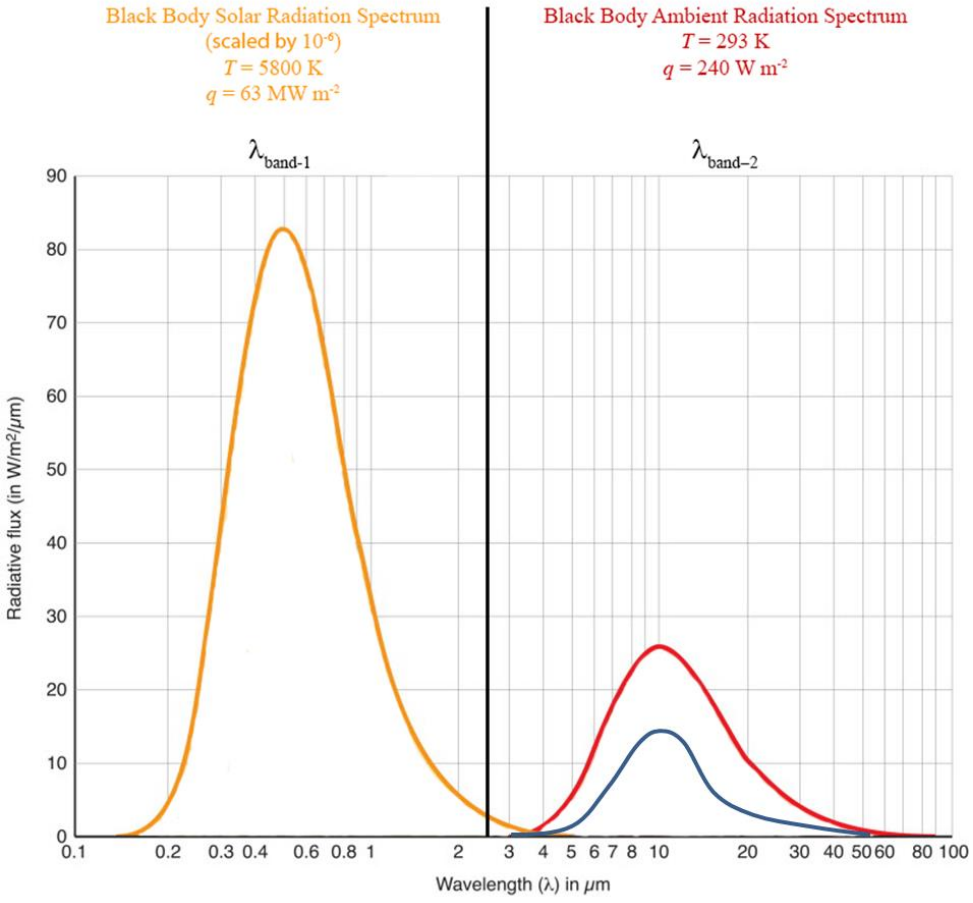

Figure 1: Blackbody radiation curves for objects at 5800 K (i.e. the sun) and 293 K (i.e. most objects on Earth), showing that hot objects emit radiation at short wavelengths and cooler objects emit radiation at longer wavelengths. Included is the radiation spectrum for an object that is also at 293 K but with a surface emissivity of 0.5 – blue curve.

However, most objects don't behave like ideal blackbodies, and emit instead some fraction of the energy of the ideal blackbody at the same temperature. This fraction (ranging from 0-1) is termed the emissivity (ε) and is a surface property. Included in Fig.1 is the radiation spectrum for a surface, also at 293 K, which has an emissivity of 0.5 (blue curve). In reality the value of the emissivity is dependent on wavelength (as well as on surface characteristics) but it is common practice to assume its value is constant over certain wavelength ranges (the so called "gray body" approximation).

In this report the radiation that is emitted by all objects other than the sun is termed 'ambient' radiation. The radiation emitted by the sun is termed 'solar' radiation. Objects on Earth (the conservatory) ***receive solar radiation but emit ambient radiation***. This is an important distinction because it renders the specification of surface emissivities for wavelengths less than 2.5 μm inappropriate, since none of the conservatory objects will reach the kind of temperatures needed to generate this type of radiation. In these instances, (i.e. for surfaces receiving solar radiation), it is much more appropriate to specify a value for the surface absorptivity (which also ranges from 0-1) which instead quantifies the fraction of the incident radiation energy that is absorbed at the surface. As the surface warms up it will continue to emit its own ambient radiation, with a radiation spectrum that depends on its temperature and the surface emissivity. For radiation emitted at these wavelengths it remains appropriate to specify a surface emissivity. The relevance of this distinction becomes more apparent in Section 4.

2.2 Reflection, Absorption and Transmission of Solar Radiation

When radiation is incident upon a surface it is reflected (ρ), absorbed (α) and transmitted (τ) in amounts that depend on the surface characteristics of the material upon which it is incident. A schematic example is shown in Fig.2, in which a quantity of energy (E_T), expressed in W/m^2, incident upon a pane of glass is partitioned into amounts of energy that are reflected, absorbed and transmitted.

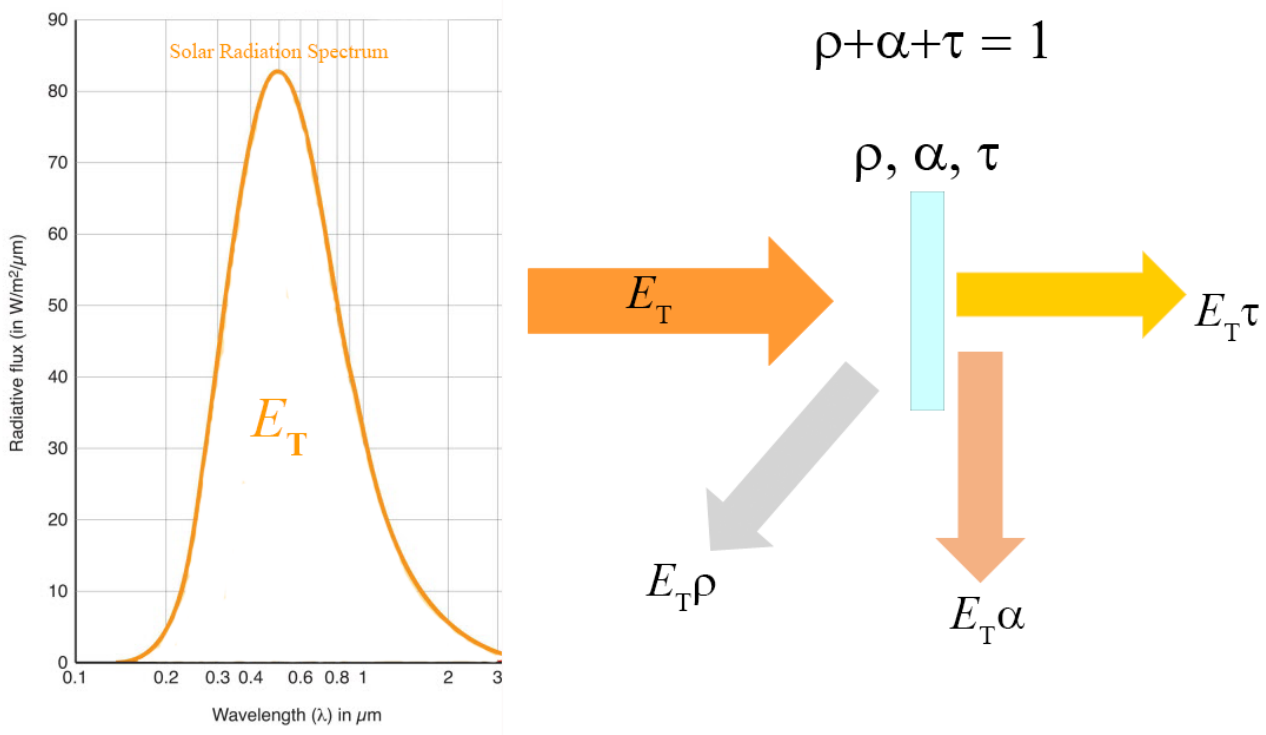

Figure 2: Schematic example of how the energy from the sun (area under the radiative flux curve – scaled in this instance by 10^{-6}) is partitioned into amounts of energy that are either reflected, absorbed or transmitted.

3 Case Study Overview

Three cases have been studied. In each case the conservatory was located in Woking (UK) had a southeast facing aspect and an elevation above sea level of 29 m. Although the sealed space width in the actual installation was 20 mm, a decision was taken by Anglian to model the installation assuming a sealed space width of 24 mm (as per Anglian's standard basic glazing specification). This does effect the window frame U-value (20% difference) but it has no effect on the levels of radiation transmission in the model and, therefore, on the levels of solar heat gain.

3.1 Case 1

The Case 1 conservatory installation had clear glazing to walls and bronze-tinted, anti-sun glazing to roof. The window pane assemblies were double glazed with the dimensions shown in Fig.3. The sealed spaces between the panes were filled with air. The 4 glazing surfaces are labelled S1-S4 from the outside surface inwards.

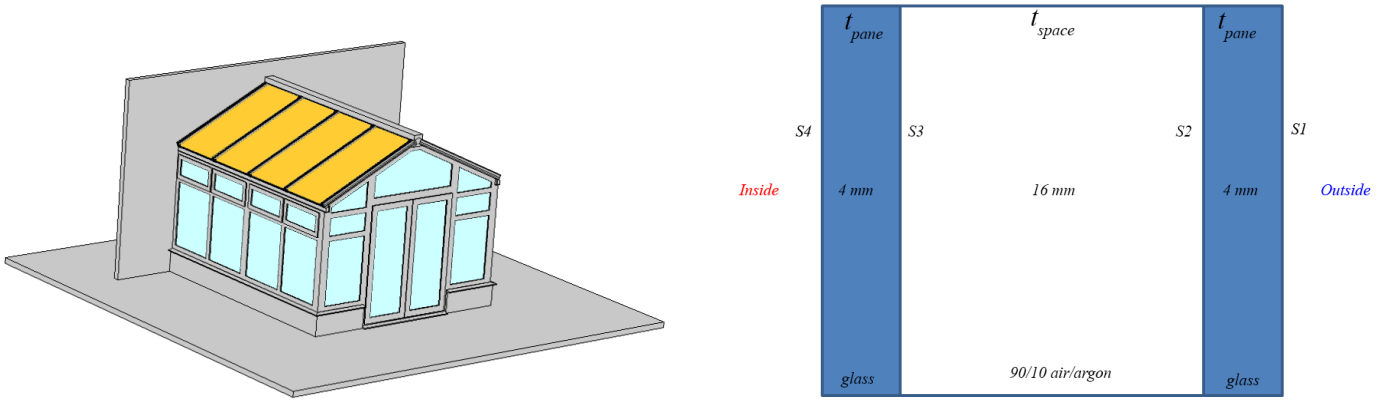

Figure 3: Case 1 conservatory installation with clear glazing to walls and bronze-tinted, anti-sun glazing to roof.

3.2 Case 2

The Case 2 conservatory had clear glazing to roof and walls. The window pane assemblies were double glazed with the dimensions shown in Fig.4. The sealed spaces between the panes were filled with air. The 4 glazing surfaces are labelled S1-S4 from the outside surface inwards.

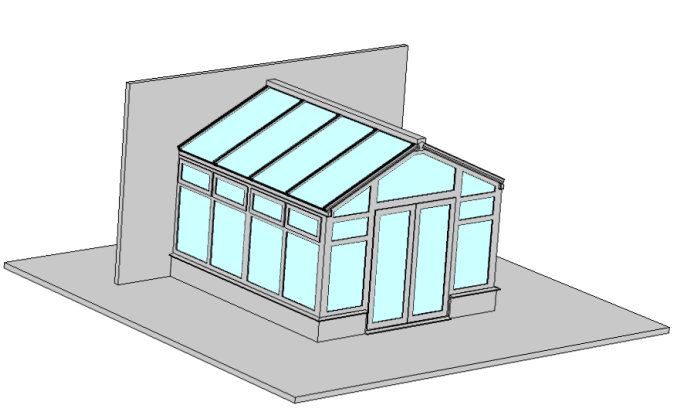

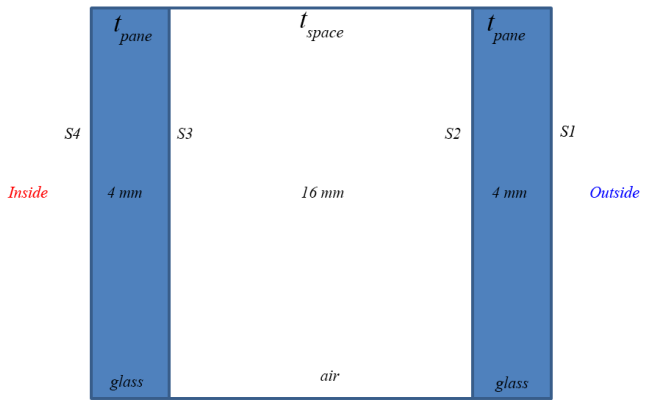

Figure 4: Case 2 conservatory installation with clear glazing to roof and walls.

3.3 Case 3

The Case 3 conservatory had SunGuard HP 50/32 to roof and SunGuard HP 60/40 to walls. The window pane assemblies were double glazed with the dimensions shown in Fig.5. The sealed spaces between the panes were filled with a 90/10 mixture of Argon/Air. The 4 glazing surfaces are labelled S1-S4 from the outside surface inwards. Surfaces S2 had a low-ε coating.

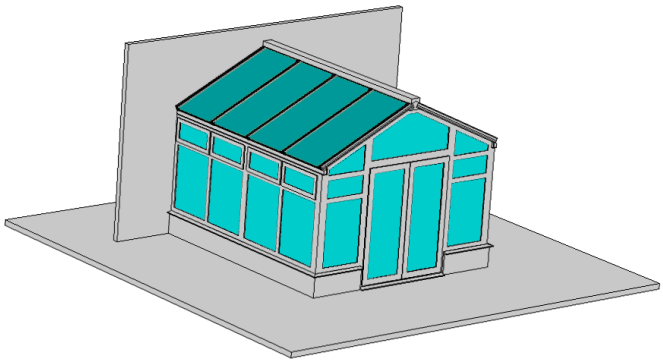

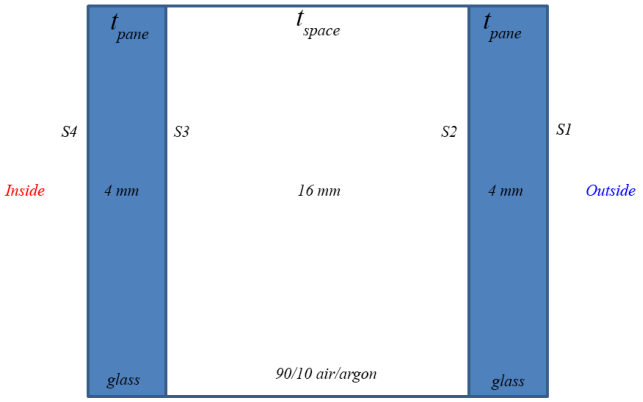

Figure 5: Case 3 conservatory installation with SunGuard HP 50/32 to roof and SunGuard HP 60/40 to walls.

4 Model Build

4.1 Geometry

The conservatory geometry was split into 12 discrete domains – Fig.6. The geometry of each domain was also simplified (to facilitate meshing and specification of boundary conditions). The simplifications were conducted in-house at Anglian, and care was taken to retain as much of the original geometry as possible so as not to (overly) compromise the validity of the model.

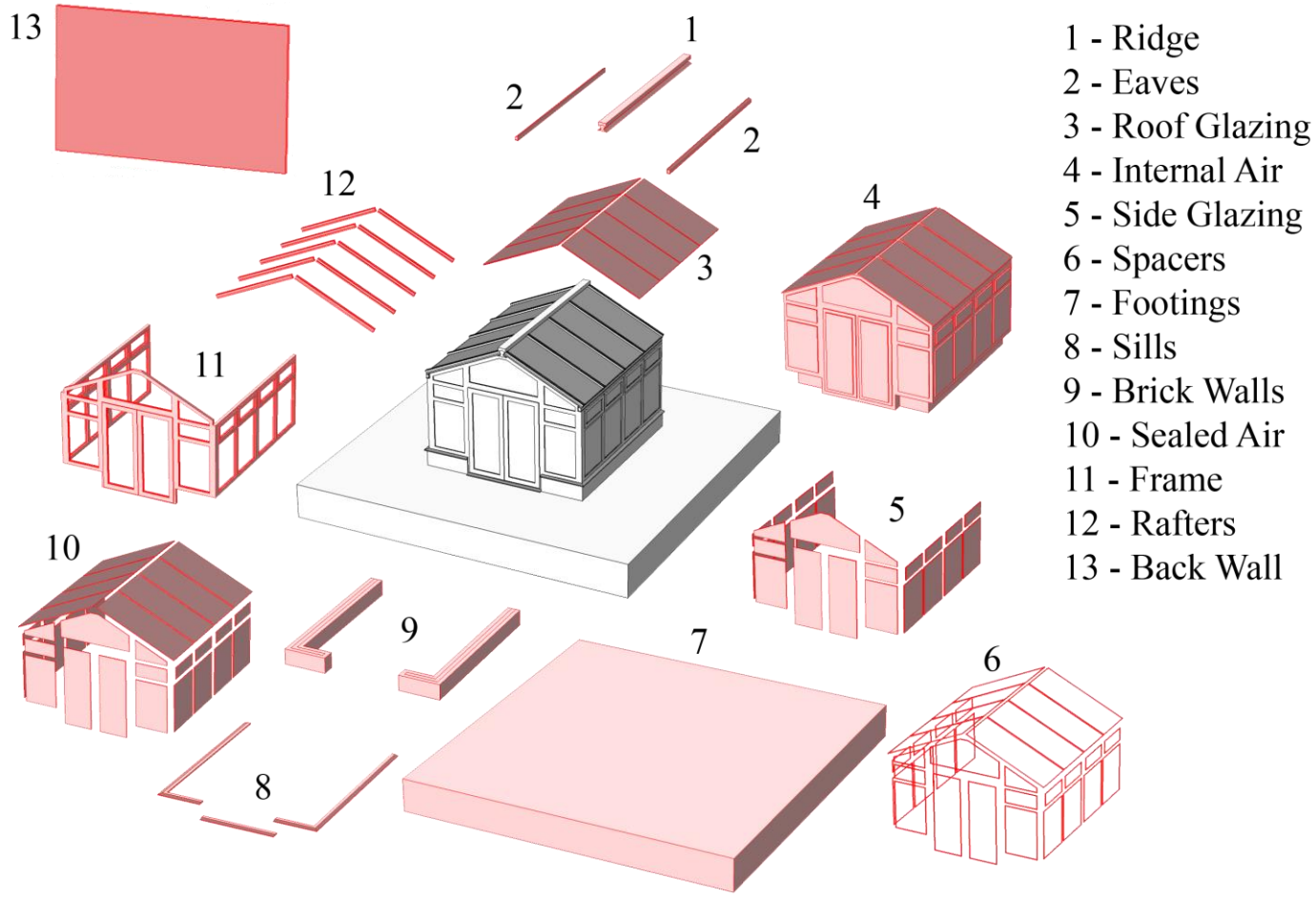

Figure 6: The full conservatory (centre) was composed of 12 discrete and geometrically simplified domains.

4.2 Geometry Simplifications

One such simplification (to the ridge component) is shown in Fig.7. The original ridge cross section is shown in Fig.7(a). The cross section geometry is relatively complex, comprising several separated chambers (plus reinforcing aluminium in the ridge, eaves and rafters, and reinforcing steel in the frame). A typical wall thickness value for the PVC is ~3 mm. The corresponding modelled (i.e. simplified) geometry is shown in Fig.7(b) in which the section is treated as being solid and absent of any reinforcing aluminium. These modifications are highly significant because they strongly affect the thermal characteristics of the component. They therefore need accounting for and a protocol for doing so can be found in Section 4.3.

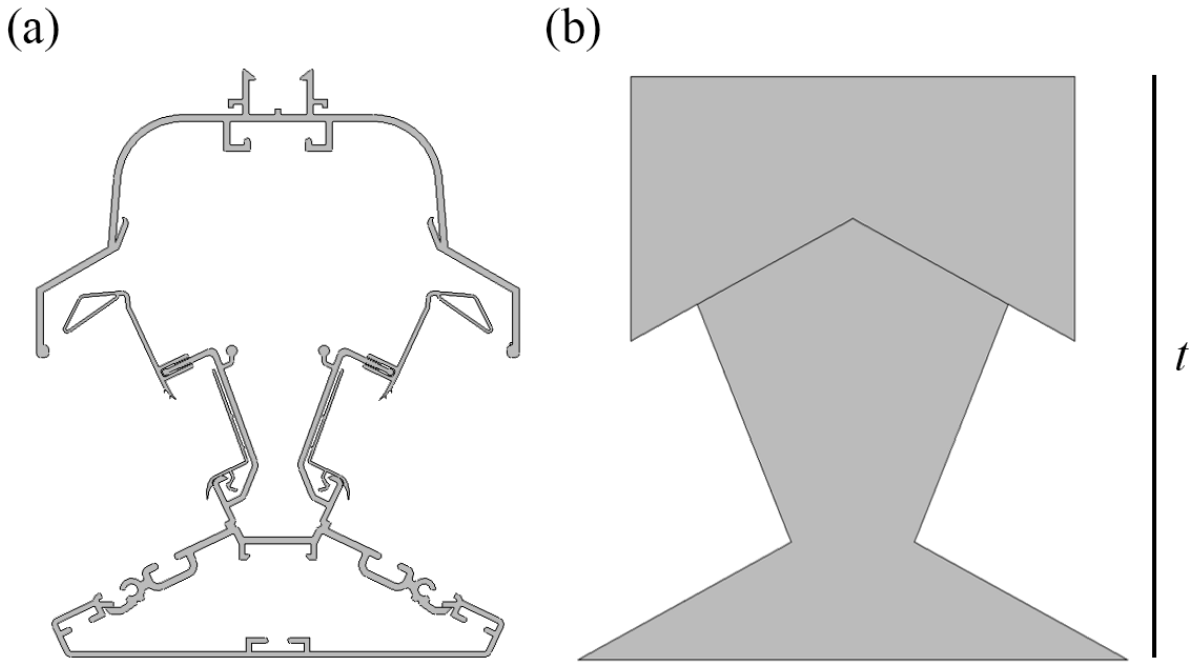

Figure 7: A cross section through the original ridge component is shown in (a). To minimise model size and complexity the component was modelled as in (b) – i.e. as a solid, simplified component. The effect on thermal characteristics was accounted for according to the protocol in Section 4.3.

4.3 A Protocol for Maintaining Component U-Values in Simplified Geometries

Consider once more the ridge component shown in Fig.7(a). The U-Value for such a component is a function of the individual thermal resistances of each of the individual elements – i.e. the PVC walls, the air gaps and any reinforcing steel that might be present. For a laminate material the U-value calculation is a trivial one (Eqn.1) but is a little more cumbersome for more complex arrangements. Nevertheless, software is available for U-value calculation of assemblies such as those in Fig.7(a) and calculated U-values for a number of the components shown in Fig.6 (and provided by Anglian) are listed in Table I [1,2]. These values include contributions from internal and external convective heat losses.

Fig.5 Component #	Component	U (W m^{-2} K^{-1})
1	Ridge	2.720
2	Eaves	3.845
11	Frame	1.549
12	Rafters	3.109
7	Footings	0.25

Table I: U-values, as calculated using Winslo2D (supplied by Anglian) for components whose geometries have been simplified. The footings U-value (blue) is the value specified by UK Building Regulations.

These U-values simply quantify the overall rate of heat transfer through assemblies like those in Fig.7(a). The U-value of the component in Fig.7(b) can be fixed at the same value as the U-value for the component in Fig.7(a) by choosing an appropriate component thickness and calculating an "equivalent" thermal conductivity using Eqn.1 (where k is thermal conductivity and t is component thickness).

$$\sum_{1}^{i} k_i / t_i \qquad (1)$$

4.4 Material Properties

Material properties for each of the 12 domains are listed in Table II. Values for the thermal conductivity of components coloured red in the table were fixed (calculated from Eqn.1) in order to maintain known component U-values (Table I) as per the protocol in Section 4.3. Values for the thermal conductivity of components coloured blue in the table were fixed (calculated from Eqn.1) to be consistent with UK Building Regulations. Densities, thermal conductivities and specific heat capacities for air and for argon had the temperature dependencies given by Eqns.2, 3 and 4.

Fig.6 #	Component	Material	K (W m^{-1} K^{-1})	C_p (J Kg^{-1} K^{-1})	ρ (Kg m^{-3})	U (W m^{-2} K^{-1})
1	Ridge	PVC	1.011	816	1400	2.720 (Table I)
2	Eaves	PVC	0.799	816	1400	3.845 (Table I)
3	Roof Glazing	Glass	1.000	730	2210	Computed
4	Internal Air	Air	Eqn.2	Eqn.3	Eqn.4	Computed
5	Side Glazing	Glass	1.000	730	2210	Computed
6	Spacers	Steel	0.350	910	2712	Computed
7	Footings	Concrete	0.160	880	2300	0.25 (B.regs)
8	Sills	PVC	0.380	816	1400	Computed
9	Brick Walls	Brick	0.500	900	2000	Computed
10	Sealed Air	Air/Argon	Eqn.2/[Eqn.2-0.0078]	Eqn.3/[Eqn.3-477]	Eqn.4	Computed
11	Frame	PVC	0.147	816	1400	1.549 (Table I)
12	Rafters	PVC	0.590	816	1400	3.109 (Table I)

Table II: Table of material properties and, where necessary, imposed U-values for geometrically simplified domains.

$$k = a + bT + cT^2 + dT^3 + dT^4 \tag{2}$$

$$C_p = e + fT + gT^2 + hT^3 + iT^4 \tag{3}$$

$$\rho = P_{abs} / RT \tag{4}$$

a	b	c	d	e	f	g	h	i	R (J/kg.K)
-0.002275	1.15E-04	-7.90E-08	4.12E-11	-7.44E-15	1047.63	-0.3725	9.45E-04	-6.02E-07	287

Table III: Equation constants for Eqns.2, 3 and 4 where T is temperature, P_{abs} is absolute pressure and R is the gas constant.

The thermal conductivity defined for the spacers (coloured green in Table II), is an area weighted value that accounts for the conductivities of the composite warm edge spacer and the polymeric seal [3]. Density, thermal conductivity and specific heat capacity values for the PVC were measured experimentally in a previous project [4].

4.5 Boundary Conditions

4.5.1 Solar Radiation

An external radiation source with solar position was specified. The specified incident solar irradiance was fixed at 1000 W m^{-2} [5], which represents the heat flux received from the sun by a surface perpendicular to its rays. For non-perpendicular surfaces the incident heat flux depends on the incident angle. The incident angle depends on the time of day, the day of the year and the geographical location of the surface.

4.5.2 Ambient Temperature Conditions

The daily ambient temperature conditions were grouped into months of the year using average monthly temperatures (maximum and minimum) for Woking, as obtained from MET office data [6]. The daily ambient temperature histories (bounded by the MET office maxima and minima) for each of the months in 2015 are shown in Fig.8. Each curve corresponds to a 24-hour period in that particular month. The green curves correspond to the months of the year that were modelled – see Section 5.

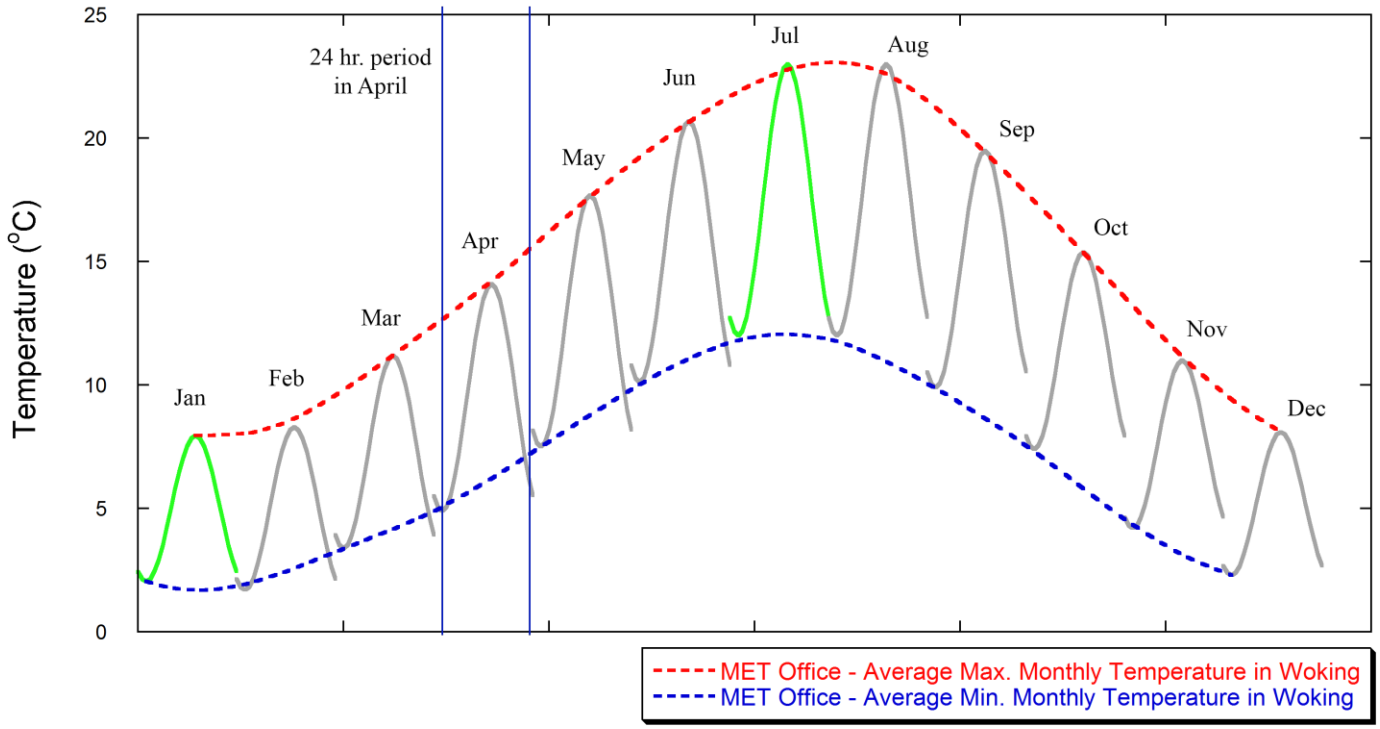

Figure 8: Daily ambient temperature histories (assumed to be the same for each day of the month), bounded by average maximum and minimum temperatures as obtained from MET office data for the Woking area.

4.5.3 Convective Heat Transfer

4.5.3.1 External

The external heat transfer coefficient was fixed on all external surfaces at 25 W m^{-2} K^{-1} as per BS EN 673:2011 for U-value calculations. The ambient (sink) temperature conditions (time of day and month of year dependent) are shown in Fig.8.

4.5.3.2 Internal

Several options were available for modelling convective heat losses from interior surfaces. One such option is to model the interior domain as a fluid and solve a fully coupled heat transfer/fluid dynamics analysis. Whilst rigorous, this method is computationally demanding whereas a simpler, more tractable approach with reasonable accuracy is to specify a Nusselt number – *Nu*. The Nusselt number simply defines the ratio between convective and conductive heat transfer normal to a surface and is given by:

$$Nu = \frac{hL}{k} = \frac{h}{k}\frac{V_{domain}}{SA_{domain}} \tag{5}$$

The Nusselt number used throughout was 660.3. It was calculated using Eqn.5, where *h* is the convective heat transfer coefficient – fixed in this instance at 7.7 W m^{-2} K^{-1} as per BS EN 673:2011, *k* is the thermal

conductivity of air 0.02 W m^{-1} K^{-1} (assumed constant and independent of *T*), and *L* is a characteristic length that, for complex shapes, is defined as the volume of the fluid domain divided by its surface area. The ambient sink temperature was set equal to the average internal room temperature (as calculated in 'real-time' by the model).

4.5.4 Radiation Heat Transfer

Surface to surface radiation boundary conditions were specified, such that all surfaces in direct view of each other and/or the sun could receive and emit radiation. The radiation received from the sun had the solar radiation characteristics shown in Fig.1. All radiation emitted by (cooler) conservatory surfaces had radiation characteristics similar to the ambient radiation spectrum, also shown in Fig.1, albeit adjusted for the actual surface temperature and the prescribed surface emissivity. Also note that, in Fig.1, the radiation incident upon the glazing surfaces has been partitioned into two distinct wavelength bands. $\lambda_{band\text{-}1}$ is the solar radiation and $\lambda_{band\text{-}2}$ is the ambient radiation wavelength range. This partitioning permits specification of a solar absorptivity in the solar wavelength band and specification of a surface emissivity in the ambient wavelength band.

4.5.4.1 Transmission of Energy

Energy, with the spectrum shown in Fig.1, is incident upon the conservatory. Total levels of incident energy are then corrected for the day and month of year, geographical location and levels of cloud cover where relevant (see Section 4.5.6). The remaining energy is then absorbed or reflected by opaque materials (frame, eaves, walls etc.) or reflected, absorbed or transmitted by semi-transparent materials (window panes). Solar absorptivities and ambient emissivities for the opaque materials are listed in Table IV. Total transmission, absorption and reflection values for complete window pane assemblies are listed in Table V. Surface emissivities (for ambient radiation) are included in the table for each of the window pane surfaces.

Component	*Absorptivity* (λ_{band_1})	*Emissivity* (λ_{band_2})	Reference
Ridge	0.77	0.90	[7]
Eaves	0.77	0.90	[7]
Footings	0.60	0.88	[8]
Sills	0.77	0.90	[7]
Brick Walls	0.65	0.93	[8]
Frame	0.77	0.90	[7]
Rafters	0.77	0.90	[7]
Conservatory Floor	0.80	0.94	[8]
Back Wall of Conservatory	0.65	0.93	[8]

Table IV: Values of surface absorptivity (for incident solar radiation) and surface emissivity (for emitted ambient radiation). All are assumed constant over their respective wavelength bands.

Double Glazing System Type	Total Transmission τ_e	Reflection ρ	Absorption α	g	Surface 1 Ambient Emissivity ε	Surface 2 Ambient Emissivity ε	Surface 3 Ambient Emissivity ε	Surface 4 Ambient Emissivity ε
Clear	0.730	0.130	0.140	0.780	0.89	0.89	0.89	0.89
Pilkington Optifloat Bronze	0.510	0.090	0.400	0.570	0.89	0.89	0.89	0.89
Sunguard HP 60/40	0.390	0.380	0.240	0.409	0.89	0.03	0.89	0.89
Sunguard HP 50/32	0.300	0.390	0.310	0.322	0.89	0.03	0.89	0.89

Table V: Values for levels of energy transmittance, reflection and absorption for each of the double glazing units plus surface emissivities for the emission of ambient radiation.

4.5.5 Underground Temperature

The temperature beneath the footings was fixed constant at 10°C which is equal to the average annual air temperature for Woking – see Fig.9 – after [10].

4.5.6 Cloud Cover

Ground-level solar irradiance levels can be strongly affected by the levels of cloud cover. To account for this, the solar irradiance level (1000 W m^{-2}) was adjusted using the cloud cover data shown in Fig.8. These data are the average recorded cloud cover levels for Woking as obtained from MET office data between 1971 and 2000. The type of cloud is not recorded, so it assumed that, for example, if 70% of the sky is covered with cloud, then the irradiance level is reduced by 70% also. Intermittent bursts of clear sky are not considered.

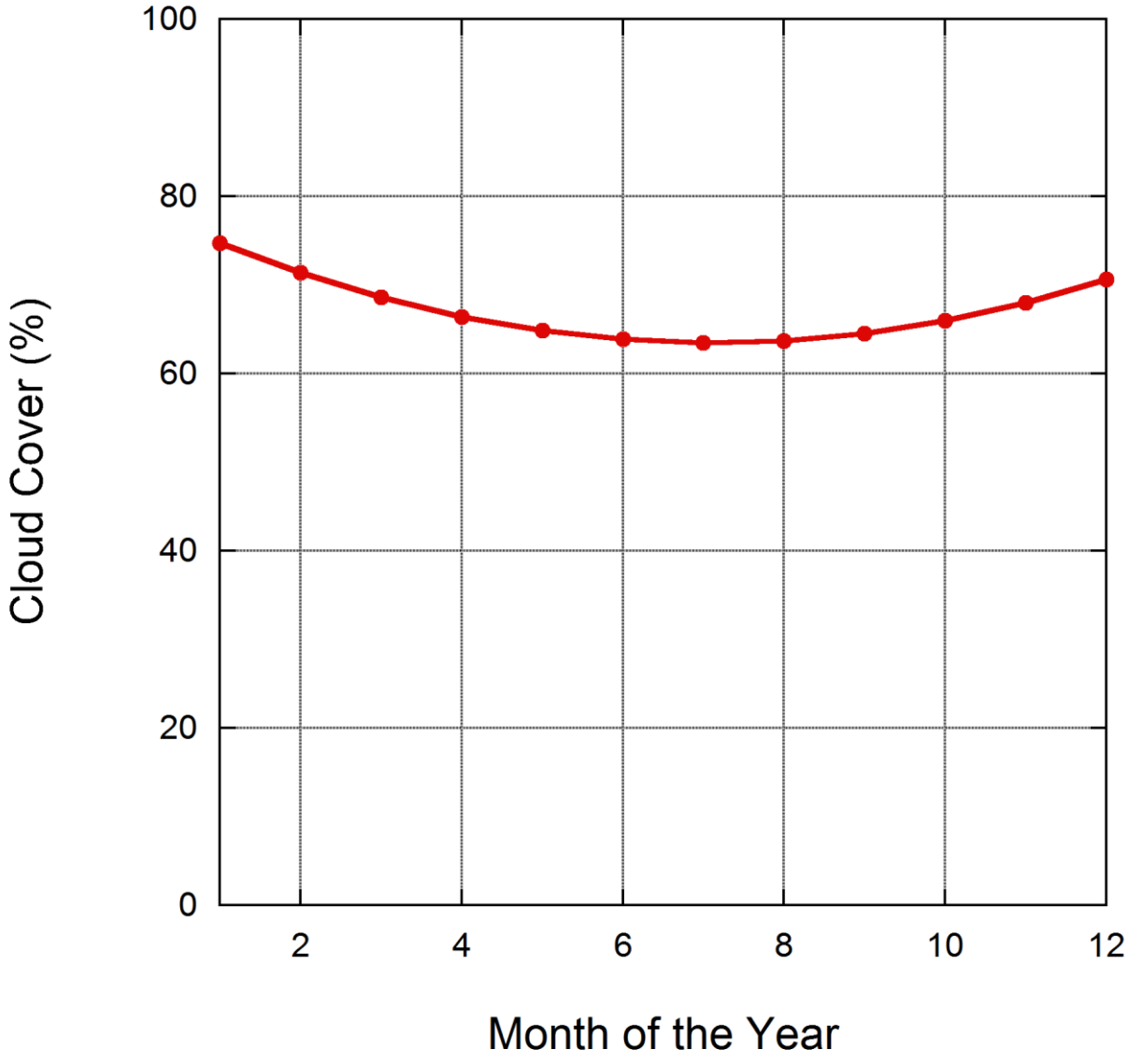

Figure 9: Average cloud cover data for Woking (measured between 1971 and 2000) obtained from MET office data.

5.0 Results

5.1 Internal Room Temperatures

Internal room temperatures for January and July are shown in Fig.10 for each of the installation types studied.

5.1.1 January

Sunrise in January (in Woking) occurs at approximately 08:00 which correlates very closely with the increase in room temperature observed in Fig.10(a). The data also show that the peak internal temperature for all three installations, which occurs at ~14:00, is below 15°C. These low temperatures are likely to feel uncomfortable so some kind of temperature control intervention would be needed (an electric heater or a radiator turned on etc.).

5.1.2 July

Sunrise in July (in Woking) occurs at approximately 05:00 which correlates very closely with the increase in room temperature observed in Fig.10(b). The data also show that the peak internal temperature for all three installations, which occurs at ~18:00, is above 35°C. These high temperatures are likely to feel uncomfortable so some kind of temperature control intervention would be needed (cooling fan, blinds, ventilation etc.).

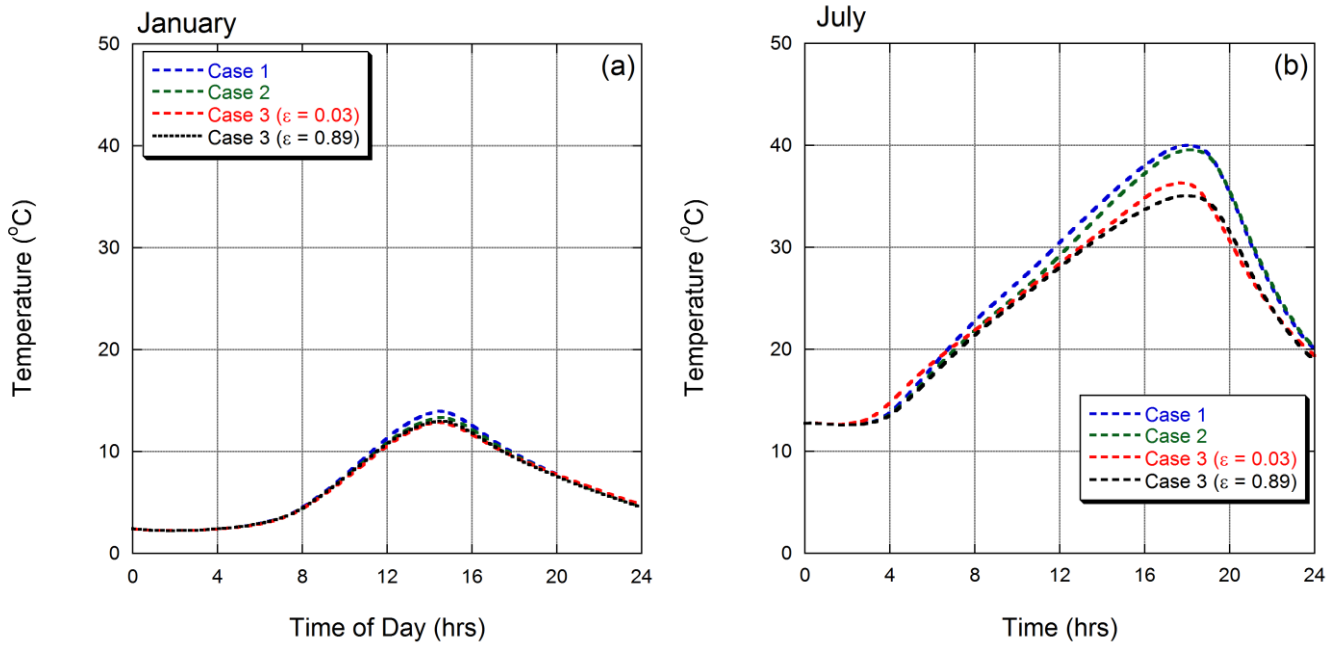

Figure 10: Predicted internal room temperatures for each of the three installation in (a) January and (b) July. Included in the figures are internal room temperatures for the Case 3 installation without the low-ε coating.

5.1.3 Internal Room Temperature Ranking

Recall that, for the Case 1 installation, the conservatory is glazed with clear glazing to sides and Pilkington Optifloat Bronze to roof. For Case 2, the conservatory is glazed with clear glazing to sides and clear glazing

to roof. The Case 3 installation is glazed with SunGuard HP 50/32 to roof and SunGuard HP 60/40 to sides. The total levels of direct solar transmission (τ_e) for each type of glazing system are given in Table V, along with their respective g-values. The glazing types are ranked in the table (highest to lowest) with respect to transmission level and g value. For instance, the data in the table show that the clear glazing has the highest transmission level (73%) and the highest g value (78%), while the SunGuard HP 50/32 has the lowest transmission level (30%) and the lowest g value (32.2%).

However, and contrary to the ranking order shown in Table V it is the Case 1 installation that attains the highest temperature in both January and July (albeit marginally). This is somewhat surprising since the total levels of direct solar transmittance (and g value) are highest for the Case 2 installation which has clear glazing to roof and clear glazing to sides. This suggests that, for the (complex) system studied, the internal temperature histories are sensitive to more than just the levels of direct solar transmission such that any prior ranking based purely on levels of transmission or g-value is likely to be inaccurate. It therefore follows that the g-value concept (while it has its merits) may, in some instances, be too simplistic to adequately capture the transient thermal behaviour of a large and 3-dimensional system containing multiple components.

For example, consider the simplified system shown in Fig.11(a). It comprises a cubic cavity, surrounded on 5 of its sides by brick with an internal lining of PVC. There is a double-glazing unit at the top of the component through which solar radiation is allowed to pass. This simplified system contains all of the physics and boundary conditions that were implemented in the full conservatory model (an ambient temperature history, incident solar radiation, radiative, conductive and convective heat transfer etc.). The internal temperature history within this simplified system is shown in Fig.11(b) for each of the glazing types listed in Table V. The ranking order is now consistent with the one in Table V, which suggests that the conservatory model set-up, and its predicted outcomes, are correct.

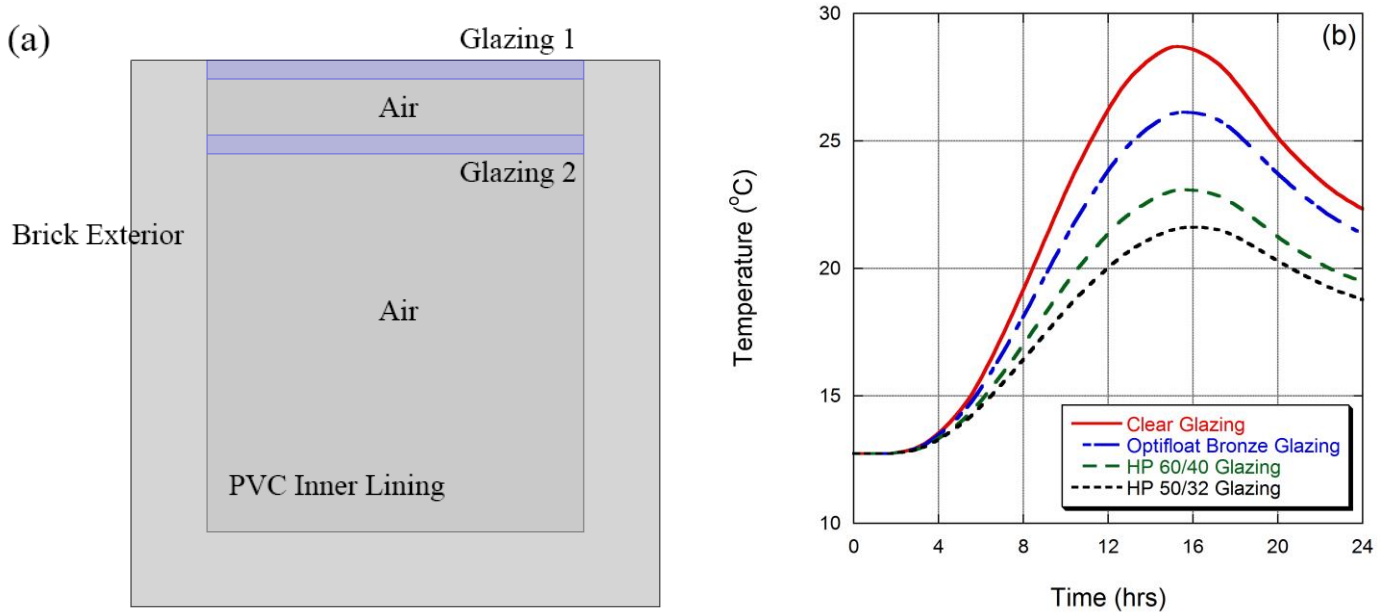

Figure 11: A schematic (2-dimensional section) of a geometrically-simplified model incorporating all of the physics and boundary conditions of the full conservatory model is shown in (a). It has been used to study how the temperatures within it vary as the glazing type is changed. The results are shown in (b).

Explanations for the difference in behaviour between this simplified system and the full conservatory might include (i) the scale and geometrical complexity of the conservatory and (ii) the fact that much of conservatory's surface area is covered in glazing since, as this proportion increases, the properties of the glazing will start to more strongly affect the behaviour of the system. For instance, Fig.12(b) plots predicted temperature histories for the three installation types where the levels of direct solar transmittance were maintained as shown in Table V, yet where all remaining solar radiation was reflected from the outer glazing surface. There was therefore no absorption of solar radiation in the glazing and, therefore, no corresponding contribution from glazing absorption on the internal temperature histories (such that the g value of the system no longer contains a contribution from the secondary internal heat transfer factor – or q_i in BS EN 410:2011). Under these conditions the Case 2 installation ***does*** attain the highest temperature – Fig.12(b). The absolute temperatures also fall markedly (by up to 5°C) from those that are shown in Fig.12(a). *(The data in Fig.12(a) are repeats of those in Fig.10(b). They are reproduced in Fig.12 to aid a direct comparison between Fig.12(a) and Fig.12(b).)*

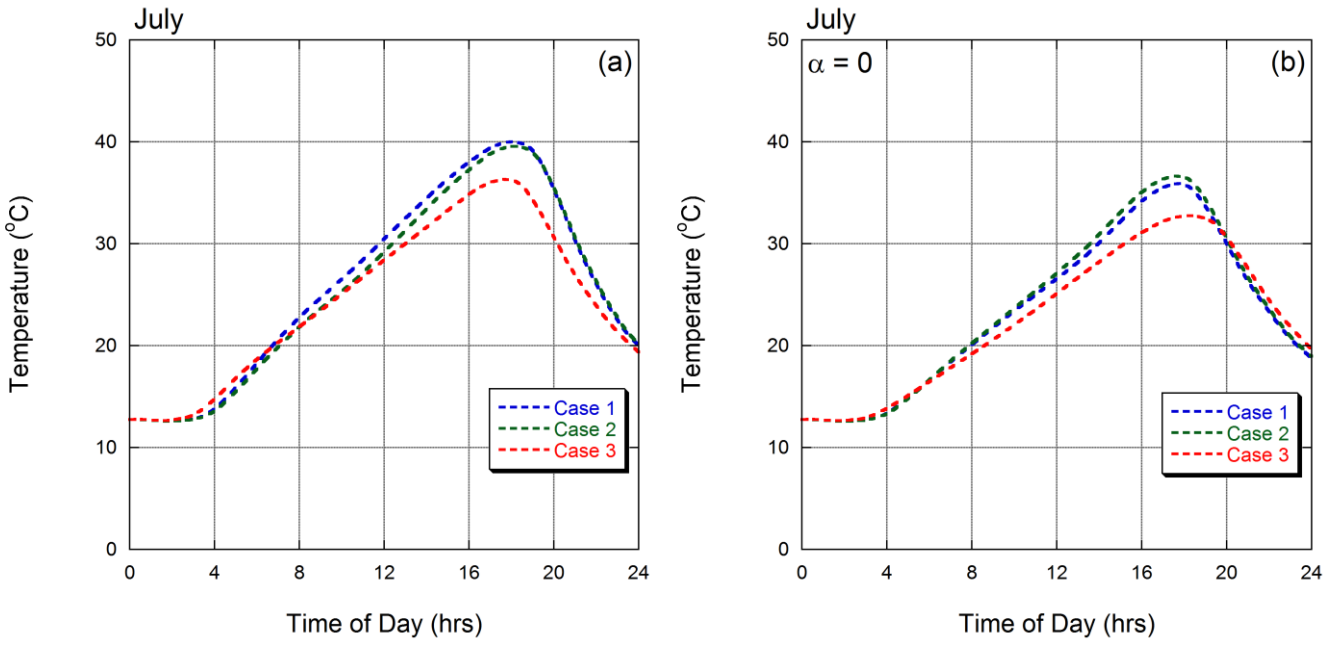

Figure 12: Predicted internal temperatures for each of the three cases when using the transmission, reflection and absorption levels given in Table V are shown in (a). In (b), the transmission levels have been kept the same but the absorption levels have been reduced to 0%.

These data demonstrate that the direct solar absorptivity of the glazing is a parameter that can significantly alter the thermal behaviour of the system and its significance is likely to become more pronounced as the proportion of glazed surface area increases. This is because high values for the direct solar absorptivity (40% in the Pilkington Optifloat Bronze) generate higher glazing temperatures which can enhance the insulating properties of glazing units. To demonstrate this point, temperature contours for the outermost and innermost surfaces of the double-glazed roofing units are shown in Fig.13 for Cases 1 and 2 at 14:00 in July. Transmission and absorption levels for the roof are shown in the figure. The contours show that the glazing surface temperatures are higher for the Case 1 installation than they are for the Case 2 installation. This is a disadvantage during summer since, if the glazing temperature (in either of the 2 panes of a double glazing unit) is greater than the internal room temperature then heat cannot escape through that unit. In fact, even if the glazing temperatures are lower than the internal room temperature the driving force for the removal

of heat will diminish as the glazing temperature rises. This enhancement of the insulating properties of the glazing unit via absorption characteristics is apparent when comparing Fig.12(a) with Fig.12(b).

To further demonstrate this point, consider Table VI which compares the average innermost surface temperature (roof glazing surface 4) with (i) the average internal room temperature and (ii) the external ambient temperature (all at 14:00 in July). The red arrows denote the corresponding direction of heat transfer with their length and number being indicative of the strength of the heat flow driving force (not to scale). The table shows that there is a stronger driving force for the removal of heat from the Case 2 conservatory installation than there is for the Case 1 installation because the temperature differences are lower for Case 1 (providing therefore a rationale for the predicted behaviour shown in Fig.10). (This analysis is somewhat simplified, since it uses average values for the temperatures which actually vary with position and with time but the principle remains unchanged.)

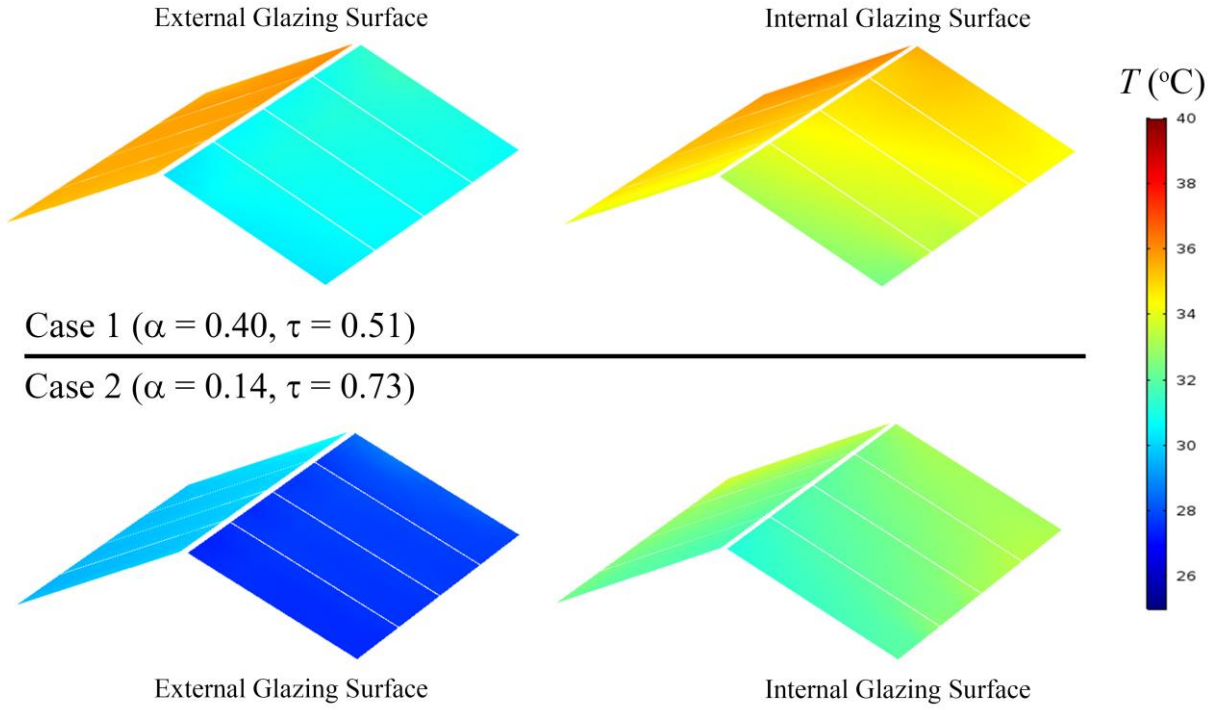

Figure 13: Predicted contours of temperature on the outer (surface 1) and inner (surface4) surfaces of the roof glazing units for Case 1 and Case 2 at 14:00 in July.

	External Ambient Temperature (°C)	Average Temperature of the Internal Roof Glazing Surface (°C)	Average Internal Room Temperature (°C)
Case 1	23	34.5	34.6
Case 2	23	32.4	33.5

Table VI: Comparison between the ambient temperature, the average internal temperature and the average temperature of the innermost surface of the roof glazing unit for Case 1 and Case 2 at 14:00 in July. The red arrows show the direction of heat flow with their length and number being indicative of the heat flow driving force (not to scale).

5.2 The Effectiveness of the Low-ε Coating

Internal room temperatures are lowest for the Case 3 installation in January and July (see Fig.10). This is unsurprising given the low levels of direct solar transmittance (τ_e) and the relatively low levels of direct solar absorptance (when compared to the Pilkington Optifloat Bronze).

Furthermore, the presence of the low-ε coating appears to have had little beneficial effect on the internal room temperature during winter. This can be seen in Fig.10(a), which plots the temperature history for the Case 3 installation with and without the low-ε coating. The temperatures in each case are almost identical. Of course, in the Case 3 installation the total levels of direct solar transmission are low, but the intention of the coating is to adequately compensate for this. One explanation for this emerges from inspection of Eqn.8, where the total (ambient) radiative heat flux from internal surfaces is given by:

$$q = \int_{\lambda \sim 2.5\,\mu m}^{\infty} \varepsilon(\lambda_{band-4})\,\sigma\left(T_{surface}^4 - T_{ambient}^4\right) d\lambda \qquad (8)$$

Eqn.8 shows that the radiative heat flux has a T^4 dependence such that the flux of emitted long wavelength radiation (i.e. the radiation that needs to be retained in order to keep the interior warm) falls markedly as the ambient (and hence the internal) temperature falls. It also falls if the difference between the temperature of emitting surfaces and the ambient temperature is low. For example, the temperature history of several internal surfaces is compared to the internal room temperature in Fig.14(a) for the Case 3 installation in January. It shows that the temperature differences between most of the surfaces and the internal temperature are small, such that the radiative heat transfer between these components and the interior of the room would also be small. In fact, two of the largest surfaces (the floor and the rear wall) are net absorbers of heat since their temperatures are lower than the ambient. One important implication of this is that the low-ε coating is probably obsolete during winter if there are no internal sources of significant levels of ambient radiation (a radiator, for instance).

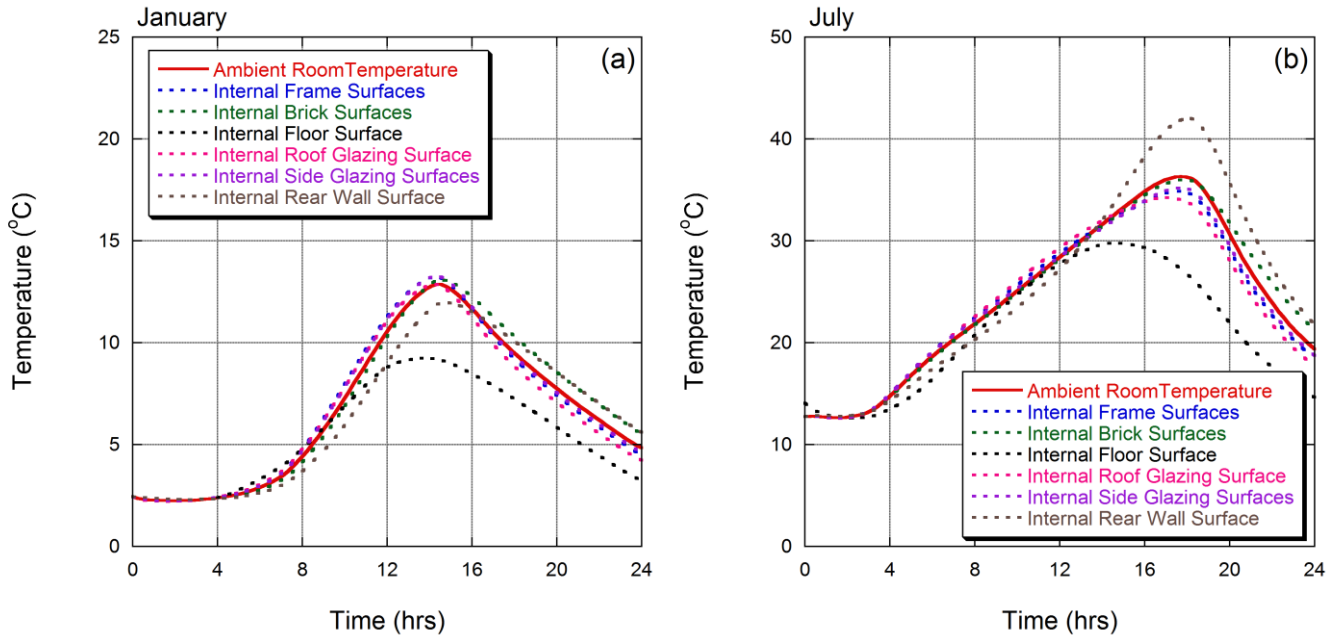

Figure 14: Predicted temperature histories (averages) for various internal surfaces for comparison with the ambient internal temperature history for (a) January and (b) July, for the Case 3 installation.

The effect of the low-e coating becomes more apparent in Fig.10(b) during summer (July) when the levels of emitted ambient radiation from internal surfaces are higher. Fig.14(b) shows that the rear wall inside the conservatory is a net emitter of ambient radiation (it is predicted to be a net absorber of heat in January). Under these circumstances the effect of the low-ε coating on the thermal behaviour is expected to become more noticeable and indeed raises the internal temperature by ~2°C in July.

5.3 Correlation with Measured Internal Temperature Data

An internal temperature of 38°C was measured inside the "real" installation (Case 3 glazing types) on August the 12th, 2014. The corresponding ambient temperature at the time of the reading was 25°C. The Case 3 model was therefore run again, this time for August 12, 2014. The simulated ambient temperature history was as shown in Fig.15. It differs a little from the temperature history shown in Fig.8 for July having been amended to account for the 25°C temperature recorded on the day (which is 2°C higher than the average temperature for that time of year).

Corresponding model predictions of the average and maximum internal temperature histories are also plotted in Fig.15(a). They show that, although the average internal temperature remains below 38°C, there are local regions within the conservatory that are hotter than 38°C. For instance, the image in Fig.15(b) shows maximum temperature fields within the conservatory at 18:00. It can be seen that the maximum internal temperatures are hottest near the rear of the conservatory and exceed 38°C. These local temperature variations and "hot-spots" depend on the position of the sun, the degree of shading, and the manner in which the heat is being diffused around the room (that could only be predicted using models of these types). The predictions also indicate that the temperature exceeds 38°C somewhere in the conservatory for at least 4 hours during the day. It is therefore unsurprising that a 38°C temperature was recorded on this day in August 2014.

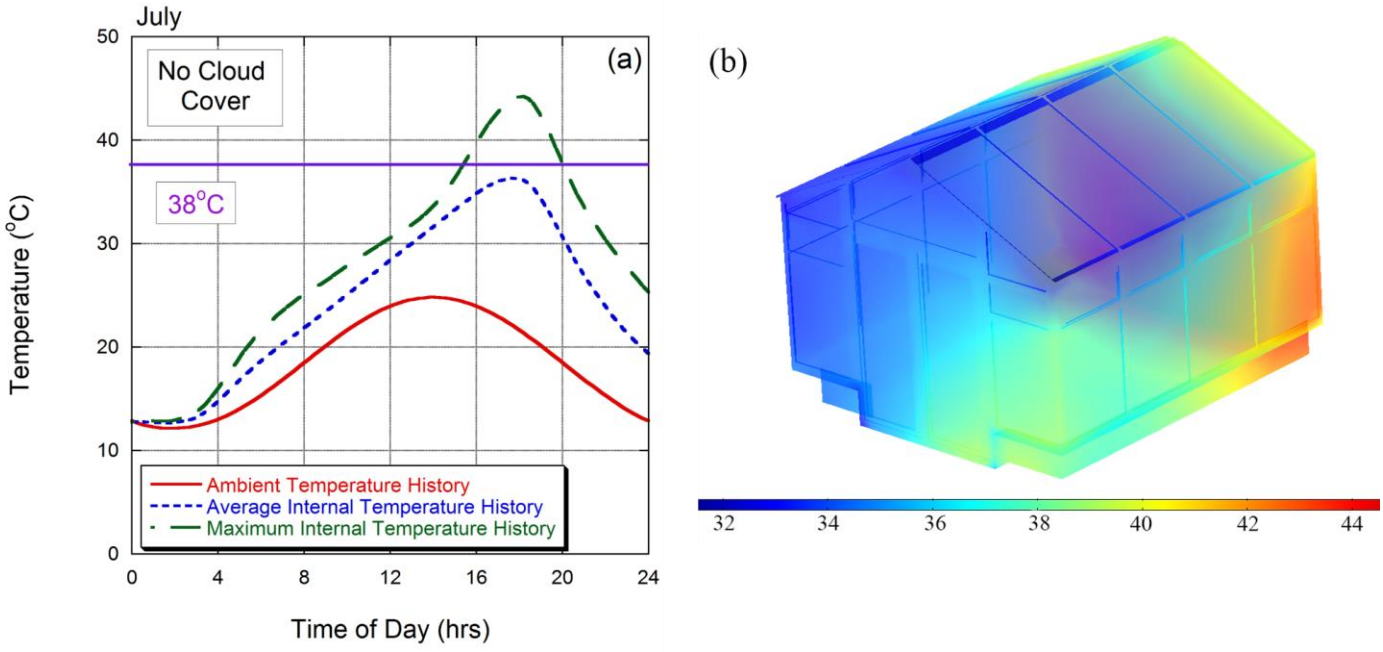

Figure 15: Predicted temperature histories (average and maximum) inside the Case 3 conservatory installation are shown in (a) along with the temperature history that was used to model the ambient temperature conditions. The maximum temperature field within the conservatory at 18:00 is shown in (b).

5.4 Cloud Cover Corrections

Predicted temperature histories are shown for each of the cases studied in Fig.16.

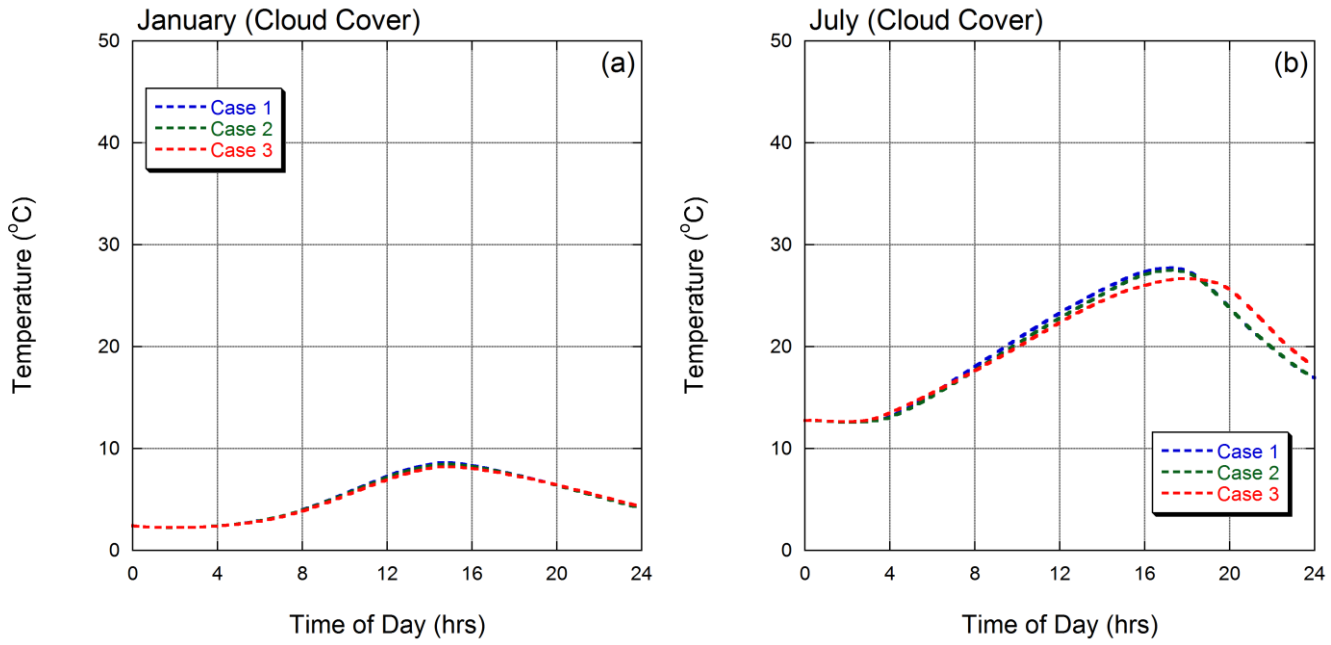

Figure 16: Predicted internal temperature histories for each of the cases studied in (a) January and (b) July when corrected for average cloud cover levels in Woking.

They were obtained by assuming the cloud cover levels shown in Fig.9. By comparing these curves to those in Fig.10 it can be seen that cloud cover levels can significantly affect the internal room temperatures. The effect in July is a positive one, with temperatures falling by more than ~6°C, although peak internal temperatures of ~27°C are still likely to be uncomfortable. The temperatures in January also fall by ~5°C, such that the degree of temperature control intervention would need to be significant to generate a comfortable temperature.

5.5 External Rafters Temperature

Maximum external surface temperatures (predicted) for each of the 5 rafters on the west facing side of the installation are plotted for July in Fig.17(a) for the Case 3 model. The data show that rafters 1 to 4 become hottest during the day, reaching ~60°C at ~2 pm. Fig.17(b) plots the rafter temperatures for the Case 1 installation. There is little difference between the curves in Fig.17(a) and Fig.17(b) which suggests that the sudden onset of peeling (that was observed) was not directly attributable to the change in glazing type.

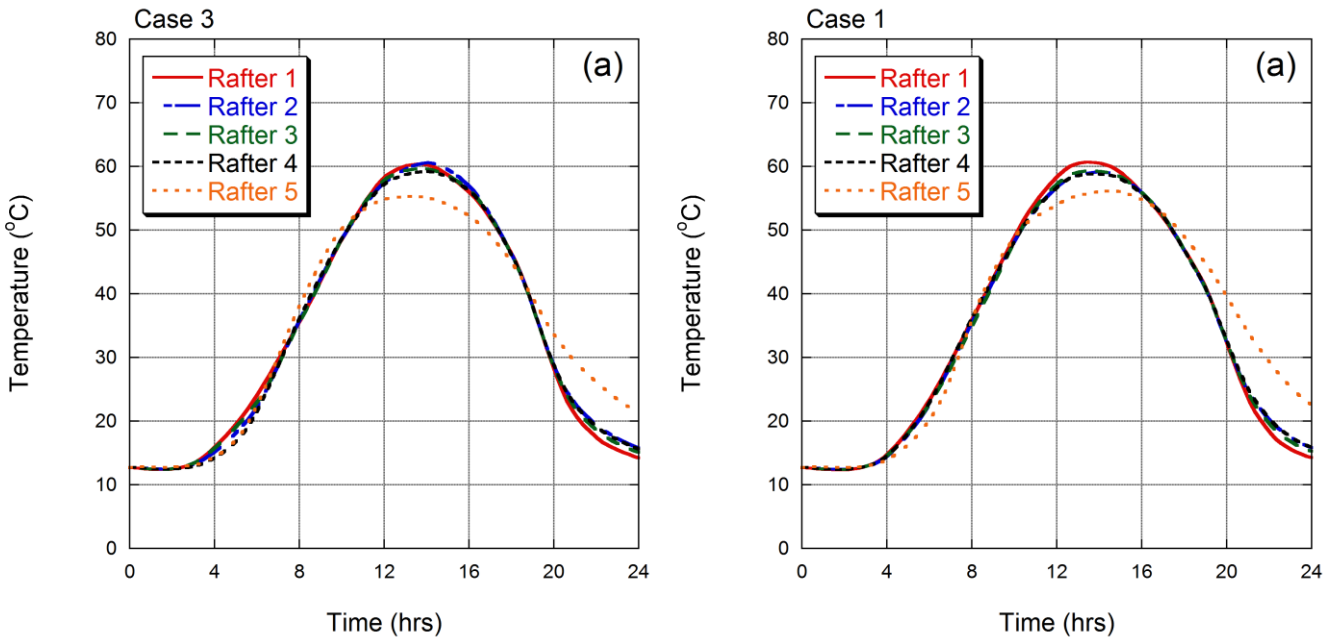

Figure 17: Predicted rafter temperatures for the Case 3 installation in June are shown in (a). Corresponding simulations are shown in (b) for the Case 1 installation

6.0 Conclusions

Finite element heat transfer analyses of a conservatory installation with a southeast facing aspect have been conducted. The original installation is in Woking and its elevation above sea level is 29 m. Three different cases were considered:

Case 1: Bronze-tinted, anti-sun glazing to the roof and clear glazing to the sides.

Case 2: Clear glazing to roof and clear glazing to sides.

Case 3: HP 50/32 glazing to roof and HP 60/40 glazing to sides. Low-ε coating applied to surface 2 of the window pane assemblies.

Internal room temperatures as a function of the time of day and month of year (January and July) were of interest, particularly in relation to the alternative glazing types used. A solar position radiative heat flux boundary condition was therefore specified, such that each of the cases were irradiated with solar radiation with an intensity and direction that depended on the time of day, the time of year and the geographical location of the installation. The following conclusions can be drawn from this work:

- Average internal room temperatures in the Case 1 and Case 2 installations are very similar, although the Case 1 internal room temperatures are marginally higher. This is despite the greater degree of direct solar transmission through the clear glazing in the Case 2 installation. This has been attributed to a higher value of the direct solar absorptivity of the Pilkington Optifloat Bronze (α = 40%) which was shown to enhance the insulating properties of the Case 1 roof glazing units. When the glazing absorptivity levels were set to 0%, the internal temperature of the Case 2 installation exceeded that of the Case 1 installation, in accordance with expectations based on g-values and levels of direct solar transmission.

- The g-value (at least when used in isolation) may be insufficient to reliably rank the transient thermal performance of conservatory (and other) installations with complex geometries containing multiple components. Although absorption characteristics of glazing units are considered in g-value calculations (via the secondary internal heat transfer factor), the calculation takes no account of the temperature difference (and hence heat flow direction) between the inner glazing surfaces and the room interior. This is a serious deficiency, since the g-value calculation assumes that the inner glazing surfaces are always net emitters of radiation when this is not necessarily the case – especially if internal room temperatures exceed inner surface glazing temperatures.
- In the absence of cloud cover, all three installations can become uncomfortably hot during peak summer months with temperatures exceeding 35°C, such that some kind of temperature control intervention would probably be required (a cooling fan, for instance).
- During winter months, and on clear days, internal room temperatures for Cases 1,2 and 3 are less than 15°C. These temperatures would clearly be uncomfortable, and would themselves require some kind of user intervention (electric heater, for instance).
- Cloud cover levels can significantly affect the internal temperature histories.
- The low-ε coating has little effect on the internal room temperature in winter. This has been attributed to low levels of ambient (long wavelength) radiation inside the conservatory. There are two reasons for this; the first is the low absolute temperatures of emitting surfaces and the second is the small difference between the temperature of the emitting surfaces and the ambient temperature.
- Heat losses are highest through the floor in winter and in summer.
- The model also shows that the external rafter temperatures remain relatively cool (peak temperatures of approximately 60°C) during peak summer months and that these temperatures are not significantly different between the Case 1 and Case 3 installations. This suggests that a change to the glazing type was not responsible for the sudden onset of peeling.
- The reliability of these model predictions would be significantly enhanced if comprehensive experimental data were available for validation purposes. In their absence these modelled data should be handled with some caution.

7.0 References

[1] Email communication with Matthew Cubitt, 19.11.15 (Email and data appended)

[2] Email communication with Matthew Cubitt, 17.11.15 (Email and data appended)

[3] Email communication with Matthew Cubitt, 17.11.15 (Email and data appended)

[4] DPC_003_Phase1_Thermal_Issue2 (copy appended)

[5] http://www.whoi.edu/science/AOPE/mvco/description/SolRad.html (last accessed 14/12/15)

[6] http://www.metoffice.gov.uk/public/weather/climate/gcpegm8xj (last accessed 11.12.15)

[7] Email communication with Julian Cubitt, 17.11.15 (Huntsman report – confidential)

[8] http://www.solarmirror.com/fom/fom-serve/cache/43.html (last accessed 14/12/15)

[9] Email communication with Matthew Cubitt, 17.11.15 (Email and data appended)

[10] Email communication with Matthew Cubitt, 16.11.15 (Email appended)